Research Article | Vol. 12, No. 6 / 1 June 2021 / Biomedical Optics Express 3597
Biomedical Optics EXPRESS

In vivo photoacoustic imaging for monitoring treatment outcome of corneal neovascularization with metformin eye drops

KWOK-HO LUI,[1,3] SHIYING LI,[1,3] WAI-SUM LO,[1] YANJUAN GU,[1] AND WING-TAK WONG[1,2,*]

[1]*Department of Applied Biology and Chemical Technology, The Hong Kong Polytechnic University, Hung Hom, Hong Kong, China*
[2]*Hong Kong Polytechnic University Shenzhen Research Institute, Shenzhen, 518057, China*
[3]*These authors contributed equally*
[*]*wing-takwong@polyu.edu.hk*

Abstract: Corneal neovascularization (CNV) compromises corneal avascularity and visual acuity. Current clinical visualization approaches are subjective and unable to provide molecular information. Photoacoustic (PA) imaging offers an objective and non-invasive way for angiogenesis investigation through hemodynamic and oxygen saturation level (sO_2) quantification. Here, we demonstrate the utility of PA and slit lamp microscope for *in vivo* rat CNV model. PA images revealed untreated corneas exhibited higher sO_2 level than treatment groups. The PA results complement with the color image obtained with slit lamp. These data suggest PA could offer an objective and non-invasive method for monitoring CNV progression and treatment outcome through the sO_2 quantification.

1. Introduction

Corneal neovascularization (CNV) is a sight-threatening condition that affects corneal avascularity in which new blood vessels grow from the limbal vascular plexus and invade cornea [1]. The transparent and avascular nature of cornea is crucial for optimal vision as well as serving as a protective mechanical barrier against foreign materials from invading ocular tissues. Under normal physiological conditions, the cornea remains a balance between the angiogenic and anti-angiogenic factors which contributes the avascular nature [2]. In this regard, studies have shown that vascular endothelial growth factor (VEGF) and soluble fms-like tyrosine kinas (sFlt) are present in human corneal epithelium [3,4]. The sFlt acts as an endogenous inhibitor which confiscates the VEGF and exhibits antiangiogenic effect to maintain corneal avascularity [4]. The disruption of this balance would lead to development of CNV, thus compromises visual acuity and structural integrity [5]. The most common causes of CNV include, but are not limited to, inflammation, trauma, bacterial/viral infection, surgery and contact lenses usage [6]. Therefore, a reliable and accurate clinical assessment is important for CNV diagnosis. Current clinical imaging techniques employ optical coherence tomography (OCT), ultrasound biomicroscope and slit lamp microscopy to examine and provide anatomical information regarding the anterior segment of the eye [7]. Color images can be taken with slit lamp microscope and undergo a computerized analysis. However, color image analysis relies on the image quality and the analysis could be subjective [8]. Furthermore, it cannot provide in-depth molecular information such as hemoglobin species and oxygen saturation (sO_2) level. Therefore, corneal angiography emerges as a valuable technique in assessing CNV and identifying blood vessels on cornea [9,10]. This technique has shown to be helpful in identifying blood vessels in the presence of corneal scaring and monitoring CNV treatment responses. Despite the advantages of angiography, it requires patients to receive injection of chemical dyes such as fluorescein or indocyanine green [10,11].

#423982 https://doi.org/10.1364/BOE.423982
Journal © 2021 Received 2 Mar 2021; revised 21 Apr 2021; accepted 21 Apr 2021; published 21 May 2021

Biomedical Optics EXPRESS

The potential adverse effects associated with chemical dye administration must not be neglected, especially for patients with liver/renal dysfunction as well as those at risk of anaphylaxis [12,13]. Therefore, there is a need to develop an objective and non-invasive imaging technique to monitor and quantify CNV progression and treatment outcome.

As an emerging noninvasive and nonionizing biomedical imaging modality, photoacoustic imaging (PAI) has drawn much attention in the past decades and has been extensively explored for potential applications in preclinical and clinical settings [14,15]. It detects the conversion of photon into acoustic pressure waves, thus providing deeper tissue penetration without compromising the spatial resolution relative to traditional optical methods. More importantly, the multiplexed PAI can be used to simultaneously visualize and differentiate multiple species with distinct absorbance profiles in a single mixture [16]. PAI has been widely employed in various biomedical research areas such as tumor detection, brain function, physiology of diseases and therapeutic monitoring based on endogenous and exogenous contrast agents [17–21]. Recently, the PAI technique has been employed to image ocular vasculature due to its advantages [22,23]. However, most studies utilize PAI for ocular vessels visualization rather than hemoglobin and sO_2 level quantification. Hemoglobin, a natural endogenous contrast agent, exists as deoxyhemoglobin (HbR) and oxyhemoglobin (HbO_2) in blood with absorption peaks at 750 and 850 nm, respectively. Hemoglobin in blood vessels acts as a strong endogenous agent in PAI which can be used to examine microvasculature and hemodynamics in biological tissues [24]. Comparing the PA signal of HbR and HbO_2 allows the calculation of sO_2 level in blood with Eq. (1) where [HbR] and [HbO_2] refer to the concentration of deoxyhemoglobin and oxyhemoglobin respectively.

$$sO_2(\%) = \frac{[HbO_2]}{[HbO_2] + [HbR]} \times 100 \tag{1}$$

The alteration of sO_2 level has shown to be associated with different types of diseases such as cancer and ophthalmic diseases [25,26]. In the field of ophthalmology, dysregulation of sO_2 level can be observed in various ocular diseases such as glaucoma and diabetic retinopathy [27–29]. Therefore, the non-invasive nature and ability to quantify sO_2 level with PAI stands out as a promising tool for monitoring CNV progression and treatment outcome.

Current clinical CNV treatment strategies can be divided into either medical or surgical intervention [30]. Surgical options include laser thermal ablation and fine needle diathermy (FND). These techniques aim at inducing immature vessels reversion and thus achieves regression of CNV [5]. Medical treatment for CNV involves the use of corticosteroid, nonsteroidal anti-inflammatory agents (NSAIDs) and anti-VEGF agents. These agents aim at demolishing angiogenic mediators for CNV associated with inflammation. Corticosteroids are often considered as the first-line treatment option owing to its anti-inflammatory and anti-angiogenic properties. However, the adverse effects associated with the long-term use of corticosteroids must not be dismissed. These adverse effects include superinfection, cataract and glaucoma [31,32]. Therefore, patients on long-term corticosteroids treatment require close monitoring for potential occurrence of adverse effects. Metformin, a hypoglycemic agent for type II diabetes, has shown to possess anti-angiogenic property in various *in vitro* and *in vivo* experimental cancer models [33–38]. Studies also revealed metformin exhibits antiangiogenic property in different ophthalmic disease models such as oxygen-induced retinopathy (OIR) and choroidal neovascularization and diabetic retinopathy (DR). However, these studies employed either intraperitoneal injection or oral gavage rather than ophthalmic administration routes [39–42] and the efficacy of metformin through ophthalmic administration routes is yet to be determined. Liu et. al. recently reported the co-delivery of metformin and levofloxacin using hydrogel is effective in treating corneal neovascularization with a single dose of subconjunctival injection [43]. To this end, we employed PAI and slit-lamp to (i) assess the efficacy of metformin eye drop against alkali-induced CNV model, (ii) monitor the *in vivo* hemodynamic status in CNV model, and (iii) quantify pre- and post-operative sO_2 level in cornea.

Biomedical Optics EXPRESS

2. Method

2.1. Materials

All chemical reagents were commercially available and used without further purification. Metformin hydrochloride ($C_4H_{11}N_5$·HCl, > 98.0%) and sodium hydroxide (NaOH, 99.99%) were obtained from Tokyo Chemical Industry Co., Ltd. and Meryer (Shanghai) Chemical Technology Co., Ltd.

2.2. Alkali-burned rat corneas and treatment

All experimental procedures complied with the Association for Research in Vision and Ophthalmology (ARVO) Statement Regarding the Use of Animals in Ophthalmic and Vision Research. The procedures were performed in accordance with the Guidelines for care and use of laboratory animals of "The Special Health Service, Department of Health, Hong Kong Special Administrative Region" and approved by the Animal Ethics Committee of "The Hong Kong Polytechnic University". Healthy adult SD rats (n = 24; Male; 200–300 g; 6–14 weeks) were employed in this study. General anesthesia was induced by 3% isoflurane inhalation followed by topical administration of 1% tropicamide (Alcon Pharmaceuticals Ltd) and tetracaine eye drops (Bausch & Lomb Pharmaceuticals, Inc) for pupil dilation and corneal surface anesthetics. A circular filter paper was soaked in 1.0 M sodium hydroxide solution and excess solution was absorbed before corneal neovascularization induction. Under a microscope, the filter paper was placed on central cornea of right eye for 30 seconds. After removal of the filter paper, the corneal surface was immediately flushed with 10 mL of PBS.

The animals were randomly divided into 4 groups (n = 6 rats/group) to receive 50 μL of saline or metformin eye drops (4 mg/mL, 40 mg/mL and 200 mg/mL) immediately after alkali-induced corneal injury. Topical administration was applied four times per day for 14 days. Eyes were examined and evaluated by slit lamp microscope before corneal injury and on 4th, 7th and 14th days after injury. Photographs were taken during examination and corneal vascularized area was analyzed automatically using ImageJ software (Wayne Rasband, National Institutes of Health, USA). The corneal neovascular area was measured in pixels and the degree of neovascularization was expressed as mean percentage ± SD.

2.3. In vivo PA imaging

Vevo LAZR Photoacoustic Imaging System (FUJIFILM VisualSonics) was used to acquire PA, Doppler and B-mode ultrasound images. The system is equipped with a tunable Nd:YAG laser system (680–980 nm, 20 Hz pulse rate, 6–8 ns pulse width, 26 mJ pulse peak energy) to trigger system acquisition and excite tissue with optical pulses to generate PA effect. The photoacoustic parameters used were: Transducer LZ-250, Frequency 21 MHz, Depth: 14.00 mm, Width: 23.04 mm, Wavelength: 750/850 nm, Threshold HbT: 20, Acquisition: sO_2/HbT. The Power Doppler sonography was recorded with a different transducer; Transducer MS-550D, Frequency 32 MHz, Pulse Repetition: 4 kHz, Depth: 10.00 mm, Width: 14.08 mm, Beam Angle: 0°, Sensitivity: 4, Wall Filter: Low. Transducers were used to acquire both photoacoustic/Doppler signal and ultrasound scans, which were later combined into one overlaid image.

At designated time points, the animals were anesthetized with 3% isoflurane and placed on a heated platform. PAI and Doppler images were recorded and acquired before and after CNV induction. Prior to the imaging process, a layer of ultrasound gel was applied over the cornea and transducer. The transducer was then aligned with cornea and laser was fired at wavelengths of 750 and 850 nm to acquire PA images. PA images (hemodynamic, oxygen saturation) and Power Doppler data were analyzed and determined with built-in oxygenation-hemoglobin measurement package in Vevo LAB (FUJIFILM VisualSonics, Toronto, Canada) workstation software. Quantification of oxygen saturation and Doppler values were done by tracing around

Biomedical Optics EXPRESS

the cornea as region of interest (ROI). The data obtained prior CNV induction will serve as baseline where the percentage change will be calculated by deducting this value. With Vevo LAB (FUJIFILM VisualSonics, Toronto, Canada) workstation software, the sO_2 values are calculated from pixels with an oxygen saturation estimate and the data are reported as average $\%sO_2$. The Doppler values are represented as percentage of vascularity calculated from the signal detected from ROI.

2.4. Histological examination

After day 14, animals were euthanized, and ocular tissues were harvested for histological examination. The eyes were fixed in 4% paraformaldehyde and sectioned for analysis. The corneal sections were then stained with CD31 and H&E followed by digital microscopy examination.

2.5. Statistical analysis

Statistical analysis was carried out in GraphPad Prism 5 software (GraphPad Software Inc.) and the data were expressed as mean ± standard deviation (SD). Differences between two groups were analyzed by the Student's t test with $*p < 0.05$ was considered statistically significant. One-way ANOVA was performed for multiple group comparisons with $*p < 0.05$ was considered statistically significant and ns presented no significance.

3. Results

3.1. Metformin reduces alkali-induced corneal neovascularization in rat cornea

The present study employed a well-established alkali-injury model to evaluate the therapeutic efficacy of metformin eye drops for CNV treatment. The representative slit-lamp images (Fig. 1(A)) indicated that newly formed blood vessels were found in the saline and metformin 4 mg/mL groups on day 4 and approached the central cornea on day 14.

Quantitative analysis revealed the vascularized area in saline-treated group markedly increased during the study period with mean area of 49.01% ± 9.42%, 51.52% ± 10.91% and 68.52% ± 9.69% on day 4, 7, and 14 respectively. Moreover, metformin 4 mg/mL group also exhibited a significant increase in vascularized area with mean area of 19.93% ± 5.75%, 35.89% ± 2.96% and 48.28% ± 11.55% on day 4, 7, and 14. It is shown that the vascularization area and severity are slightly lower with metformin 4 mg/mL group when compared with saline-treated group.

Upon increasing the concentration by 10- and 50-fold, metformin significantly inhibited angiogenesis with a mild increase in newly formed vessels on day 4 and the growth was maintained at low level throughout the study periods. Quantitative analysis revealed both groups exhibited similar vascularization area with mean vascularization area of 12.72% ± 5.47%, 6.325% ± 0.61% and 2.25% ± 0.61% on day 4, 7, and 14 respectively.

The CNV inhibitory effect of topically applied metformin was investigated with histological examination using H & E and CD 31 staining (Fig. 1(B) and 1(C)). Neo-vessels can be observed in saline-treated and metformin 4 mg/mL group while no obvious vessels can be noted in metformin 40 mg/mL and metformin 200 mg/mL treated group. The number of microvessels in corneal tissue sections stained with CD31 demonstrate the anti-angiogenesis effect of metformin. The microvessel density in metformin 40 mg/mL and 200 mg/mL treated group significantly decreased as compared to the saline and metformin 4 mg/mL treated group. Therefore, the histological examination indicated topical administration of metformin is effective in inhibiting CNV with an optimal concentration of 40 mg/mL.

Biomedical Optics EXPRESS

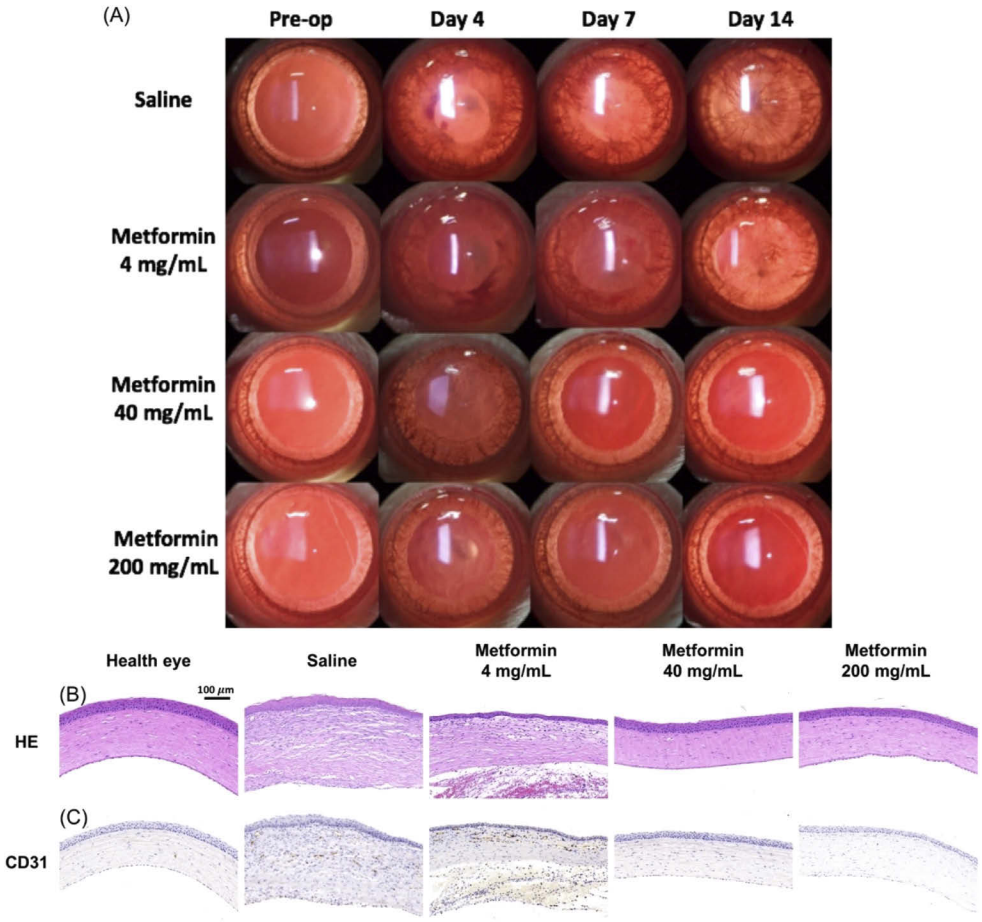

Fig. 1. Inhibition of alkali-induced CNV with metformin eye drop. (A) Representative slit lam images of pre- and post-treatment with different metformin concentration. Representative (B) H&E and (C) CD31 staining images (scale bar for Fig. 1 B and 1 C = 100 μm) in different treatment groups on Day 14.

3.2. Change of corneal hemodyamic after alkali-induced corneal neovascularization

Photoacoustic imaging (PAI) was utilized to monitor and assess the hemodynamic change before and after CNV induction. We first employed PAI to record and investigate the change of HbO_2 and HbR which correspond to the wavelengths of 850 and 750 nm respectively.

Prior to CNV induction, all animal subjects show a low baseline PAI signal in their corneas. After the alkali injury was inflicted on cornea, we observed a significant increase in PAI signal of HbO_2 and HbR (Fig. 2(A)) in saline and metformin 4 mg/mL treatment group. Quantitative analysis (Fig. 2(B)) revealed that there was an 8.80-fold increase (0.44 ± 0.12) in HbR signal compared to the baseline (0.05 ± 0.0013) in saline group on day 4. The HbR signal exhibited a slight regression on day 7 (0.38 ± 0.044) and 14 (0.29 ± 0.013) respectively. A similar trend can be observed in HbO_2 signal (Fig. 2(C)) in saline group with an 8.97-fold increase (0.61 ± 0.14) on day 4 and remained at a similar level (0.65 ± 0.022) on day 7 followed by a slight regression (0.54 ± 0.037) on day14.

The metformin 4 mg/mL treatment group also exhibited an increasing trend in HbR signal with a 3.07-fold (0.23 ± 0.018) increase on day 4 compared with the baseline value (0.075 ± 0.0016).

Biomedical Optics EXPRESS

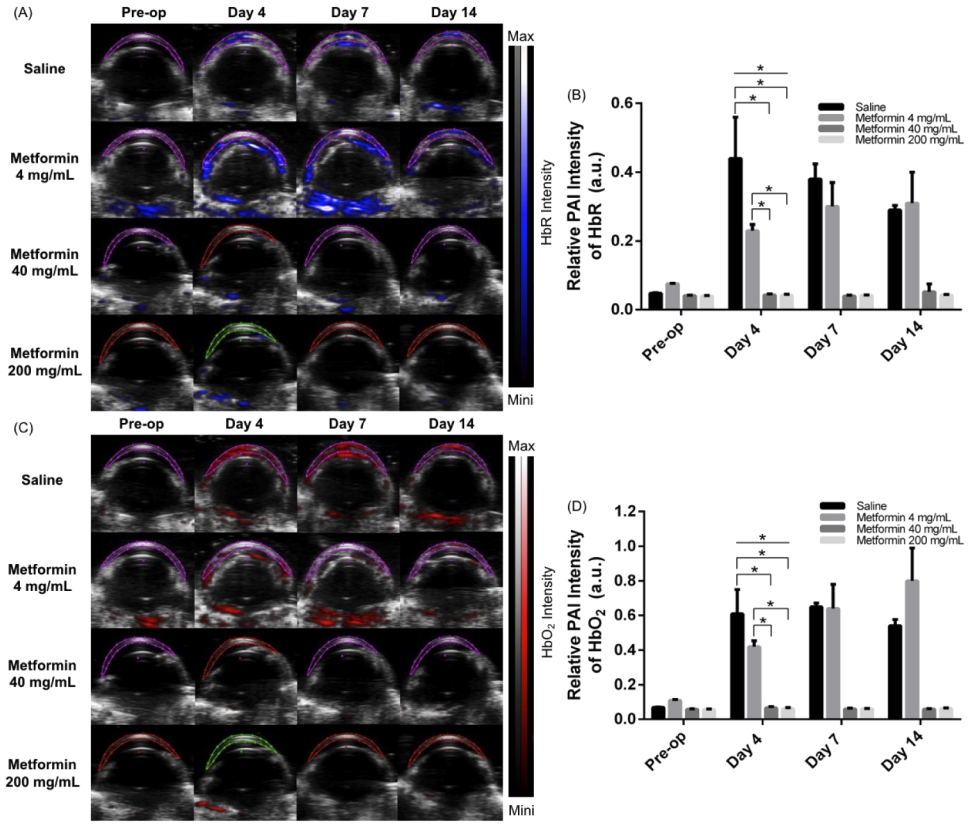

Fig. 2. Co-registered PA and ultrasound images for hemodynamic status. (A) Pre- and Post-operative *in vivo* PA intensity of HbR (Blue color). (C) Pre- and Post-operative *in vivo* PA intensity of HbO_2 (Red color). Relative PA intensity of (B) HbR and (D) HbO_2. $*p < 0.05$.

The HbR signal remained at a similar level on day 7 (0.30 ± 0.07) and day 14 (0.31 ± 0.09) respectively. Similarly, HbO_2 signal also showed a 3.8-fold increase (0.42 ± 0.034) on day 4 when compared with the baseline value (0.11 ± 0.0046). The HbO_2 PAI signal further increased with a factor of 5.81 (0.64 ± 0.14) and 7.27 (0.8 ± 0.19) on day 7 and day 14 respectively.

However, rat received metformin 40 mg/mL and 200 mg/mL remained similar corneal HbO_2 and HbR PAI signal throughout the study period. Thus, this indicated its efficacy in inhibiting CNV progression.

3.3. Change of $\%sO_2$ in cornea after corneal neovascularization

Once we confirmed PAI was capable of measuring HbR and HbO_2 in corneas, we utilized the built-in sO_2 mode to examine the corneal oxygen saturation level and the data are shown as average $\%sO_2$. Figure 3(A) shows the co-registered PA and ultrasound images for the change of $\%sO_2$ before and after CNV induction. Quantitative analysis (Fig. 3(B)) revealed that saline and metformin 4 mg/mL treatment group exhibited a significant increase in average $\%sO_2$ on day 4, 7 and 14. The average $\%sO_2$ in saline group reached 46.82% ± 6.12, 51.04% ± 1.97 and 40.09% ± 5.71 on day 4, 7 and 14 respectively. The metformin 4 mg/mL group also showed a similar average $\%sO_2$ pattern with 24.07% ± 5.22, 57.47% ± 6.94 and 45.47% ± 7.40 on day 4, 7 and 14 respectively. In contrast, the metformin 40 mg/mL and 200 mg/mL groups showed a subtle

Biomedical Optics EXPRESS

increase in the average $\%sO_2$ with 0.21% ± 0.15 and 0.08% ± 0.20 on day 4 respectively. The average $\%sO_2$ levels subsequently returned to pre-stimulation level on day 7 and 14.

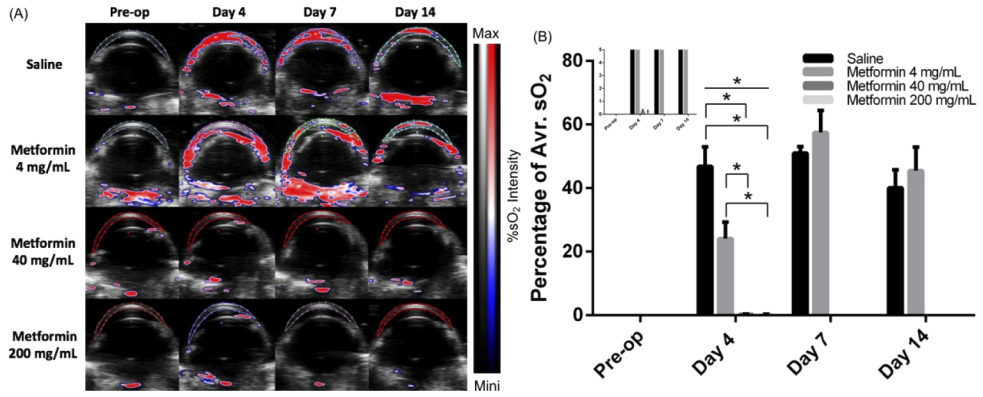

Fig. 3. Co-registered PA and ultrasound images for $\%sO_2$ in cornea. (A) Pre- and Post-operative *in vivo* PA imaging for $\%sO_2$ with different treatment groups. (B) Relative PA intensity of $\%sO_2$. $*p < 0.05$.

3.4. Doppler sonography

We next measured the blood flow across the corneas using Power Doppler mode to assess the percentage of vascularity over the study period. Doppler sonography revealed an increase in percentage of vascularity in saline and metformin 4 mg/mL treatment group after alkali-injury (Fig. 4). Our data suggested that the saline group exhibited 4.24% ± 0.38 increase on day 4 and reached 15.95% ± 0.51 on day 7 followed by a reduction (11.85% ± 1.6) on day 14. The metformin 4 mg/mL group showed an increase in signal from 3.73% ± 0.73 on day 4 to 9.12% ± 2.32 and 12.41% ± 1.47 on day 7 and day 14 respectively. However, the metformin 40 mg/mL and 200 mg/mL groups remained at pre-treatment level after corneal neovascularization with exception of a slight increase on day 4. In agreement with the $\%sO_2$ data, Doppler sonography revealed an increasing trend after corneal neovascularization induction in saline and metformin 4 mg/mL group.

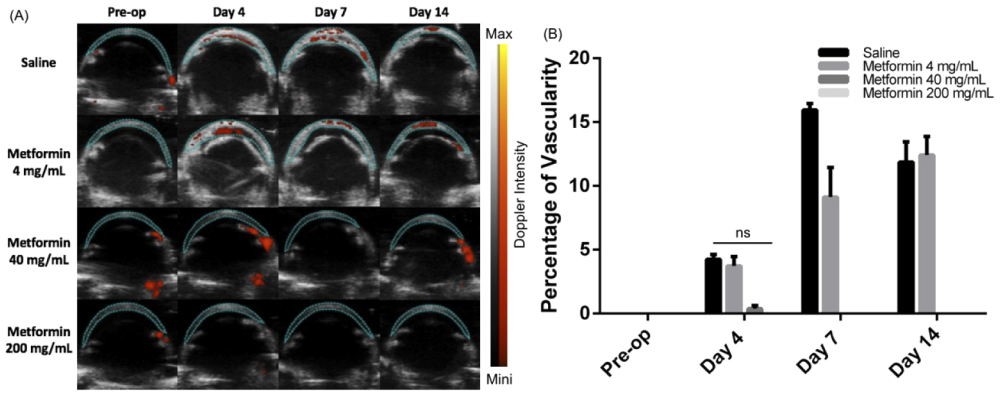

Fig. 4. Co-registered Doppler and ultrasound images for change of blood vascularity. (A) Pre- and Post-operative *in vivo* PA imaging for percentage change of vascularity with different treatment groups. (B) Relative Doppler intensity of vascularity change. ns = no significance.

Biomedical Optics EXPRESS

4. Discussion and conclusion

Coupling with slit lamp microscope and PAI modality, our data demonstrated the efficacy of metformin eye drop against CNV. Slit lamp images have shown improvement upon topical administration of metformin when compare with saline-treated group. Quantitative analysis with color images revealed a significant increase in corneal neovascularization area in saline-treated group. However, color images analysis can be subjective and does not offer any molecular insights of the disease progression. Furthermore, the cornea's dome shape makes it difficult to focus and capture all blood vessels in one single clear image [44]. In addition, the presence of scarring leads to difficulty in visualizing blood vessels from color images [10]. Therefore, the image quality hinders the reliability of color image analysis. Herein, we applied a non-invasive PAI technique to monitor various parameters to assess the disease progression and treatment outcome. We investigated the change of hemodynamic status, $\%sO_2$ change and Doppler blood flow. The data obtained was then quantified to provide in-depth molecular information regarding the disease progression. Unlikely other tissues, a healthy cornea possesses an avascular feature in order to provide an optimal vision. However, with alkali-injury, our data have shown increases in hemodynamic status, $\%sO_2$ and Doppler vascularity in saline group and metformin 4 mg/mL group. Consistent with the color images, saline-treated diseased eye exhibited higher $\%sO_2$ level and Doppler vascularity than metformin 40 mg/ml and 200 mg/ml treatment group. The increase in these signals are complementary with each other and thus validate the hemodynamic changes measured following the CNV induction. PAI also offers unique advantages over traditional fluorescent angiography techniques as it does not require any use of exogenous contrast agents. This technique relies on natural endogenous contrast agents, HbO_2 and HbR, which exists within cornea during diseased condition. Moreover, the measurement of hemoglobin contents and the sO_2 level could provide in-depth molecular insights regarding the disease progression and offer a quantitative assessment of CNV. Furthermore, the PAI can by-pass the obstacles with slit lamp evaluation and avoid potential subjective bias in color image analysis, therefore allowing PAI to act as an objective, label-free and non-invasive tool for disease monitoring. Despite the promising features of PAI, potential laser impact on ocular functionalities after longitudinal usage must not be negligible. Further experiment and evaluation are warranted to ensure the safety of PAI after longitudinal ocular examination.

In our study, we employed topical administration as it is the most convenient and non-invasive ophthalmic administration route for ocular diseases treatment [45,46]. However, the unique anatomical structure of cornea hinders the drug absorption and often results in poor bioavailability profile. Studies have shown that up to 95% of topically applied drug is lost due to various defense mechanisms such as tear turnover, reflex blinking and solution drainage [47]. In our work, we investigated three difference concentrations and found that the optimal concentration is 40 mg/mL for CNV treatment. Our data suggested that concentration higher than 40 mg/mL does not seem to provide any significant improvement. Though this study does not emphasize the underlying mechanism, numerous researches have indicated the anti-angiogenic properties of metformin. Studies have suggested that metformin reduces and inhibits vascular endothelial growth factor (VEGF) receptor Flk-1 level, expression of activin receptor-like kinase 1 (ALK1) as well as VEGF-A protein translation in different ophthalmic diseases models [39–41]. Furthermore, metformin exhibits anti-inflammatory properties which reduces inflammatory cytokines such as interleukin-6 (IL-6) and monocyte chemotactic protein-1 (MCP-1) [42].

In summary, we demonstrated the utility of PAI modality and slit lamp to monitor and assess the therapeutic efficacy of metformin eye drops for CNV treatment. Our data suggested that metformin eye drop with concentration of 40 mg/mL is effective in inhibiting CNV progression. By investigating various parameters, the PAI technique could provide comprehensive molecular information regarding the disease status. Therefore, this technique would be useful to assess treatment outcome and exhibit great potential in monitoring post-operative blood vessels growth

Biomedical Optics EXPRESS

after cornea transplantation. Given its capability to reveal molecular insights, this reinforces its potential application on ocular disease assessment using PAI technique. Therefore, the unique advantages of PAI technique enable it to act as a non-invasive and label-free tool for longitudinal monitoring of ocular diseases provided that it does not have any negative impacts on long-term ocular functionalities.

Funding. Hong Kong Polytechnic University (Area of Excellence Grants (1-ZVGG)).

Acknowledgement. We would like to acknowledge the use of The Hong Kong Polytechnic University [University Research Facility for Chemical and Environmental Analysis (UCEA) and University Research Facility in Life Science (ULS)].

Disclosures. The authors declare no conflicts of interest.

Data availability. Data underlying the results presented in this paper are not publicly available at this time but may be obtained from the authors upon reasonable request.

References

1. J.-H. Chang, N. K. Garg, E. Lunde, K.-Y. Han, S. Jain, and D. T. Azar, "Corneal neovascularization: an anti-VEGF therapy review," Surv. Ophthalmol. **57**(5), 415–429 (2012).
2. N. S. Abdelfattah, M. Amgad, A. A. Zayed, H. Hussein, and N. A. El-Baky, "Molecular underpinnings of corneal angiogenesis: advances over the past decade," Int. J. Ophthalmol. **9**(5), 768 (2016).
3. G. B. Setten, "Vascular endothelial growth factor (VEGF) in normal human corneal epithelium: Detection and physiological importance," Acta Ophthalmol. Scand. **75**(6), 649–652 (2009).
4. B. K. Ambati, E. Patterson, P. Jani, C. Jenkins, E. Higgins, N. Singh, T. Suthar, N. Vira, K. Smith, and R. Caldwell, "Soluble vascular endothelial growth factor receptor-1 contributes to the corneal antiangiogenic barrier," Br. J. Ophthalmol. **91**(4), 505–508 (2007).
5. Z. Sharif and W. Sharif, "Corneal neovascularization: updates on pathophysiology, investigations & management," rjo **63**(1), 15–22 (2019).
6. N. S. Abdelfattah, M. Amgad, A. A. Zayed, H. Salem, A. E. Elkhanany, H. Hussein, and N. A. El-Baky, "Clinical correlates of common corneal neovascular diseases: a literature review," Int. J. Ophthalmol. **8**(1), 182–193 (2015).
7. K. P. Kubelick, E. J. Snider, C. R. Ethier, and S. Emelianov, "Photoacoustic properties of anterior ocular tissues," J. Biomed. Opt. **24**(05), 1 (2019).
8. W. Liu, K. M. Schultz, K. Zhang, A. Sasman, F. Gao, T. Kume, and H. F. Zhang, "In vivo corneal neovascularization imaging by optical-resolution photoacoustic microscopy," Photoacoustics **2**(2), 81–86 (2014).
9. S. B. Kirwan, P. Ruaidhrí, Y. Zheng, A. Tey, D. Anigeet, and H. Sueke, "Quantifying changes in corneal neovascularization using fluorescein and indocyanine green angiography," Am. J. Ophthalmol. **154**(5), 850–858.e2 (2012).
10. D. R. Anijeet, Y. Zheng, A. Tey, M. Hodson, H. Sueke, and S. B. Kaye, "Imaging and evaluation of corneal vascularization using fluorescein and indocyanine green angiography," Invest. Ophthalmol. Visual Sci. **53**(2), 650–658 (2012).
11. N. Spiteri, V. Romano, Y. Zheng, S. Yadav, R. Dwivedi, J. Chen, S. Ahmad, C. E. Willoughby, and S. B. Kaye, "Corneal angiography for guiding and evaluating fine-needle diathermy treatment of corneal neovascularization," Ophthalmology **122**(6), 1079–1084 (2015).
12. T. W. Olsen, "Anaphylactic shock following indocyanine green angiography," Arch. Ophthalmol. **114**(1), 97 (1996).
13. S. Bearelly, S. Rao, and S. Fekrat, "Anaphylaxis following intravenous fluorescein angiography in a vitreoretinal clinic: report of 4 cases," Can. J. Ophthalmol. **44**(4), 444–445 (2009).
14. C. Kim, C. Favazza, and L. V. Wang, "In vivo photoacoustic tomography of chemicals: high-resolution functional and molecular optical imaging at new depths," Chem. Rev. **110**(5), 2756–2782 (2010).
15. J. Weber, P. C. Beard, and S. E. Bohndiek, "Contrast agents for molecular photoacoustic imaging," Nat. Methods **13**(8), 639–650 (2016).
16. A. Taruttis and V. Ntziachristos, "Advances in real-time multispectral optoacoustic imaging and its applications," Nat. Photonics **9**(4), 219–227 (2015).
17. J. Levi, S. Kothapalli, S. Bohndiek, J.-K. Yoon, A. Dragulescu-Andrasi, C. Nielsen, A. Tisma, S. Bodapati, G. Gowrishankar, X. Yan, C. Chan, D. Starcevic, and S. S. Gambhir, "Molecular photoacoustic imaging of follicular thyroid carcinoma," Clin. Cancer Res. **19**(6), 1494–1502 (2013).
18. C. Xie, X. Zhen, Y. Lyu, and K. Pu, "Nanoparticle regrowth enhances photoacoustic signals of semiconducting macromolecular probe for in vivo imaging," Adv. Mater. **29**(44), 1703693 (2017).
19. Q. Chen, C. Liang, X. Sun, J. Chen, Z. Yang, H. Zhao, L. Feng, and Z. Liu, "H_2O_2 -responsive liposomal nanoprobe for photoacoustic inflammation imaging and tumor theranostics via in vivo chromogenic assay," Proc. Natl. Acad. Sci. U. S. A. **114**(21), 5343–5348 (2017).
20. J. Laufer, P. Johnson, E. Zhang, B. Treeby, B. Cox, B. Pedley, and P. Beard, "In vivo preclinical photoacoustic imaging of tumor vasculature development and therapy vasculature development and therapy," J. Biomed. Opt. **17**(5), 1 (2012).

Biomedical Optics EXPRESS

21. X. Yang, S. E. Skrabalak, Z. Li, Y. Xia, and L. V. Wang, "Photoacoustic tomography of a rat cerebral cortex in vivo with au nanocages as an optical contrast agent," Nano Lett. **7**(12), 3798–3802 (2007).
22. S. Jeon, H. B. Song, J. Kim, B. J. Lee, R. Managuli, J. H. Kim, J. H. Kim, and C. Kim, "In vivo photoacoustic imaging of anterior ocular vasculature: a random sample consensus approach," Sci. Rep. **7**(1), 4318 (2017).
23. W. Liu and H. F. Zhang, "Photoacoustic imaging of the eye: a mini review," Photoacoustics **4**(3), 112–123 (2016).
24. L. J. Rich and M. Seshadri, "Photoacoustic monitoring of tumor and normal tissue response to radiation," Sci. Rep. **6**(1), 21237 (2016).
25. M.-L. Li, J.-T. Oh, X. Xie, G. Ku, W. Wang, C. Li, G. Lungu, G. Stoica, and L. V. Wang, "Simultaneous molecular and hypoxia imaging of brain tumors in vivo using spectroscopic photoacoustic tomography," Proc. IEEE **96**(3), 481–489 (2008).
26. A. Hariri, J. Wang, Y. Kim, A. Jhunjhunwala, D. L. Chao, and J. V. Jokerst, "In vivo photoacoustic imaging of chorioretinal oxygen gradients," J. Biomed. Opt. **23**(03), 1 (2018).
27. E. Vandewalle, L. Abegão Pinto, O. B. Olafsdottir, E. De Clerck, P. Stalmans, J. Van Calster, T. Zeyen, E. Stefánsson, and I. Stalmans, "Oximetry in glaucoma: correlation of metabolic change with structural and functional damage," Acta Ophthalmol. **92**(2), 105–110 (2014).
28. O. B. Olafsdottir, S. H. Hardarson, M. S. Gottfredsdottir, A. Harris, and E. Stefa, "Retinal oximetry in primary open-angle glaucoma," Invest. Ophthalmol. Visual Sci. **52**(9), 6409–6413 (2011).
29. S. H. Hardarson and E. Stefasson, "Retinal oxygen saturation is altered in diabetic retinopathy," Br. J. Ophthalmol. **96**(4), 560–563 (2012).
30. D. Roshandel, M. Eslani, A. Baradaran-Rafii, A. Y. Cheung, K. Kurji, S. Jabbehdari, A. Maiz, S. Jalali, A. R. Djalilian, and E. J. Holland, "Current and emerging therapies for corneal neovascularization," Ocul. Surf. **16**(4), 398–414 (2018).
31. D. Gupta and C. Illingworth, "Treatments for Corneal Neovascularization: A Review," Cornea **30**(8), 927–938 (2011).
32. S. Feizi, A. A. Azari, and S. Safapour, "Therapeutic approaches for corneal neovascularization," Eye Vis. **4**(1), 28 (2017).
33. H. Qu and X. Yang, "Metformin inhibits angiogenesis induced by interaction of hepatocellular carcinoma with hepatic stellate cells," Cell Biochem. Biophys. **71**(2), 931–936 (2015).
34. Y. Yang, G. Jin, H. Liu, K. Liu, J. Zhao, X. Chen, D. Wang, R. Bai, X. Li, Y. Jang, J. Lu, Y. Xing, and Z. Dong, "Metformin inhibits esophageal squamous cell carcinoma-induced angiogenesis by suppressing JAK/STAT3 signaling pathway," Oncotarget **8**(43), 74673–74687 (2017).
35. R. Rattan, R. P. Graham, J. L. Maguire, S. Giri, and V. Shridhar, "Metformin suppresses ovarian cancer growth and metastasis with enhancement of cisplatin," Neoplasia **13**(5), 483–IN28 (2011).
36. J. Wang, X. Sun, Q. Ma, L. Cong, H. Zhang, D. Fan, J. Feng, S. Lu, J.-L. Liu, G.-Y. Li, and P.-J. Liu, "Metformin's antitumour and anti-angiogenic activities are mediated by skewing macrophage polarization," J Cell Mol Med **22**(8), 3825–3836 (2018).
37. J. Wang, G. Li, Y. Wang, S. Tang, X. Sun, X. Feng, Y. Li, G. Bao, P. Li, X. Mao, M. Wang, and P. Liu, "Suppression of tumor angiogenesis by metformin treatment via a mechanism linked to targeting of HER2/HIF-1α/VEGF secretion axis," Oncotarget **6**(42), 44579–44592 (2015).
38. S. Orecchioni, F. Reggiani, G. Talarico, P. Mancuso, A. Calleri, G. Gregato, V. Labanca, D. M. Noonan, K. Dallaglio, A. Albini, and F. Bertolini, "The biguanides metformin and phenformin inhibit angiogenesis, local and metastatic growth of breast cancer by targeting both neoplastic and microenvironment cells," Int. J. Cancer **136**(6), E534–E544 (2015).
39. S. G. Joe, Y. H. Yoon, J. A. Choi, and J. Koh, "Anti-angiogenic effect of metformin in mouse oxygen-induced retinopathy is mediated by reducing levels of the vascular endothelial growth factor receptor Flk-1," PLoS One **10**(3), e0119708 (2015).
40. Y. Ying, T. Ueta, S. Jiang, H. Lin, Y. Wang, D. Vavvas, R. Wen, Y.-G. Chen, and Z. Luo, "Metformin inhibits ALK1-mediated angiogenesis via activation of AMPK," Oncotarget **8**(20), 32794–32806 (2017).
41. Y. Zhang, F. Chen, and L. Wang, "Metformin inhibits development of diabetic retinopathy through microRNA-497a-5p," Am. J. Transl. Res. **9**(12), 5558–5566 (2017).
42. J. Han, Y. Li, X. Liu, T. Zhou, H. Sun, P. Edwards, H. Gao, Y. Fu-Shin, and Q. Xiaoxi, "Metformin suppresses retinal angiogenesis and inflammation in vitro and in vivo," PLoS One **13**(3), e0193031 (2018).
43. D. Liu, Q. Wu, Y. Zhu, Y. Liu, X. Xie, S. Li, H. Lin, W. Chen, and F. Zhu, "Co-delivery of metformin and levofloxacin hydrochloride using biodegradable thermosensitive hydrogel for the treatment of corneal neovascularization," Drug Deliv. **26**(1), 522–531 (2019).
44. L. A. Faraj, D. G. Said, and H. S. Dua, "Evaluation of corneal neovascularisation," Br. J. Ophthalmol. **95**(10), 1343–1344 (2011).
45. K. Cholkar, S. P. Patel, A. D. Vadlapudi, and A. K. Mitra, "Novel strategies for anterior segment ocular drug delivery," J. Ocul. Pharmacol. Ther. **29**(2), 106–123 (2013).
46. A. Patel, "Ocular drug delivery systems: an overview," WJP **2**(2), 47 (2013).
47. R. Gaudana, H. K. Ananthula, A. Parenky, and A. K. Mitra, "Ocular drug delivery," AAPS J **12**(3), 348–360 (2010).